# First-principles study of high-temperature phases of $K_2SeO_4$

Razvan Caracas* and Xavier Gonze
*Unité de Physico-Chimie et de Physique de Matériaux, Université Catholique de Louvain, place Croix du Sud 1, B-1348 Louvain-la-Neuve, Belgium*

(Received 4 July 2006; published 16 November 2006)

We study from first principles the electronic, structural, dielectric, and dynamical properties of the hexagonal and orthorhombic structures of $K_2SeO_4$. The two ideally ordered high-$T$ hexagonal phases are a model for many other phases of this compound, obtained by slight distortions of these highly symmetric structures. We determine the lattice and atomic parameters of these phases, and describe their band structure. All the structures present zone-center dynamical instabilities. We compare the zone-center vibrational frequencies with the available experimental data.

DOI: 10.1103/PhysRevB.74.195111 PACS number(s): 71.20.−b, 77.22.−d, 61.66.−f, 63.20.Dj

## I. INTRODUCTION

$K_2SeO_4$ is the archetypal material for a large family of compounds with general formulas $A_2BX_4$ and $ABCX_4$, exhibiting a rich sequence of phase transitions at low temperatures, with normal, commensurate and incommensurate structures.[1–4] All these structures originate from slight distortions of a (disordered) hexagonal phase. Such a hexagonal phase has been experimentally identified only in $K_2SeO_4$ and $K_2SO_4$ at high temperatures. In the other materials, e.g., $Rb_2ZnBr_4$, (Ref. 5), $Rb_2ZnCl_4$ (Ref. 6), the melting point is lower than the hypothetical phase transition temperature. At room temperature, most of these materials exhibit an orthorhombic structure, which under further cooling transforms to an incommensurately modulated (IC) structure. At low temperature, the modulation wave vector locks in: the structure is commensurately modulated. Other low-symmetry structures, orthorhombic, monoclinic, and triclinic, have been reported for several compounds upon further cooling.[7–9]

The experimental studies of the high-temperature hexagonal phase (phase I), of $K_2SeO_4$ (Refs. 10–12) focused on the determination of the space group and ordering state of the structure. These data are consistent with the $\alpha$-$K_2SO_4$ structure ($P6_3/mmc$ space group). According to the apex model, adopted hereafter, the $SeO_4$ tetrahedra exhibit an orientational disorder, pointing independently up and down with respect to the hexagonal $c$ axis. The hexagonal lattice constant have been measured, while information on the internal degrees of freedom is lacking.

Upon cooling, the hexagonal structure transforms to an orthorhombic phase (phase II) at 545 K. This orthorhombic phase presents a soft-mode behavior, and transforms at 130 K to an incommensurately modulated structure, phase III, with a modulation wave vector $\mathbf{q}=\langle 1/3(1-\delta)00\rangle$, where $\delta$ has a small incommensurate value.[13] The incommensurate structure presents a lock-in behavior, and transforms at 93 K to another orthorhombic phase, phase IV, that presents a $3a\times b\times c$ superstructure of the phase II.

Most theoretical studies focused on the normal-incommensurate-commensurate transitions. We find it useful to briefly survey them now, even if our paper focuses on the normal high-temperature phases. In these studies, empirical and/or semiempirical potentials (with one exception, Ref. 14 based on a Gordon-Kim model) were used to describe the dynamics of the phase transitions: neither the ground-state features, nor the hexagonal structures are discussed. A Landau-Ginzburg model is used in Ref. 15 to examine the phase transitions where the predicted commensurate-incommensurate transition temperature is higher than the measured one. A phenomenological competing interaction model is built and analyzed in Ref. 8, and phase transition diagrams, depending on different parameters, are built. Born-Mayer-type semiempirical potentials with parameters fitted to static data are used[16–18] to simulate the dynamics of the phase transitions. The normal-incommensurate theoretical transition temperature agrees well with the experimental ones. The soft mode results from the interaction of an optical branch with a transverse acoustic branch. Molecular dynamics simulations,[19] using a potential with point charge Coulombic and short-range repulsive forces, lead to the correct disorder and space group for the high-$T$ hexagonal structure. However, no structural details, like atomic positions, are provided, and the incommensurate phase is also not simulated. Monte Carlo investigations are performed in Ref. 20 using an Ising-type model, with interaction constants calculated on the basis of the electrostatic model. The calculations agree with the experimental data, and the existence of a short-wavelength modulation in the incommensurate phase, not observed in experiments, is predicted. The lattice dynamics analysis of $K_2SeO_4$, using a rigid-ion model with the selenate groups reduced to rigid bodies,[21] reproduces semiquantitavely the phonon dynamics, and the soft-mode behavior. The electronic band structure was reported previously,[22] but as a result of semiempirical linear combination of atomic orbitals (LCAO) calculations.

In view of the previous theoretical studies, we consider that an *ab initio* approach is needed to improve the understanding of the physics responsible for the complex behavior of these materials. Here, we report results from first-principles calculations, using the local density approximation (LDA) within the density functional theory (DFT): analysis of the electronic, structural, dielectric, and zone-center dynamical properties, of phases I and II, and phonon band structure of phase I, which constitute a mandatory step before the *ab initio* study of lower temperature phases of $K_2SeO_4$ and related compounds.

 

The paper is organized as follows. Section II describes the computational methodology. The electronic properties, the valence electron distribution, the electronic band structure, and the electronic density-of-states are discussed in Sec. III. We show that $K_2SeO_4$ is an insulator with a 3.67 eV 0 K-LDA gap. The structure is build from isolated K cations and anionic $SeO_4$ tetrahedral groups. The results of the structural determination for both the orthorhombic and hexagonal phase are presented in Sec. IV. We determine two ideally ordered hexagonal structures, with the $SeO_4$ tetrahedra pointing in the same direction and in opposite directions, providing detailed structural data. We analyze the dielectric properties, the dielectric tensor, and the Born effective charges in Sec. V. Section VI presents the zone-center dynamical properties. The first hexagonal structure, with the tetrahedra pointing in the same direction, exhibits two unstable modes at $\mathbf{q}(0\ 0\ 0)$, dominated by rotations of the $SeO_4$ tetrahedra around [110] directions, and the second hexagonal structure, with the tetrahedra pointing in different directions, exhibits only one such unstable mode, dominated by rotations of the $SeO_4$ tetrahedra and displacements of the K atoms parallel to the Cartesian axes. The orthorhombic structure presents two instabilities in $\mathbf{q}(0\ 0\ 0)$. The agreement with the experimental frequencies for the Raman and infrared modes of the orthorhombic structure is discussed. In Sec. VII, we analyze the phonon band structure of the two hexagonal structures. The different low-temperature structures (including the orthorhombic one) can be obtained by the condensation of the unstable phonons at the zone center, or in the whole Brillouin zone. The paper ends with the conclusions.

## II. COMPUTATIONAL METHODOLOGY

All the calculations are based on the local density approximation (LDA) of the density functional theory (DFT).[23,24] We use the ABINIT package.[25,26] The ABINIT software is based on plane waves and pseudopotentials. The three elements are represented by Troullier-Martins pseudopotentials.[27] The considered valence electrons for K, Se, and O are $3p^6 4s^1$, $4s^2 4p^4$, and $2s^2 2p^4$, respectively. The occupation of the electronic levels is determined by the Fermi-Dirac statistics, with a temperature of 0 Kelvin.

The structural relaxation was conducted using the Broyden-Fletcher-Goldfarb-Shanno minimization,[28] modified to take into account the total energy as well as the gradients.

The dynamical matrices, Born effective charges and dielectric permittivity tensors, were computed within density-functional perturbation theory, using the responses to atomic displacements and homogeneous electric fields.[29–32]

## III. STRUCTURAL DETERMINATION

### A. Hexagonal structure

The hexagonal disordered phase of $K_2SeO_4$ has a $P6_3/mmc$ space group (on average) and $Z=2$. The $SeO_4$ tetrahedra may be found in two possible orientations: pointing up or down the $c$ hexagonal axis. By combining these two possible states and taking into account possible symmetries, we obtain two ideal ordered structures, that describe the two extreme cases of the disordered state. In the first case, the two tetrahedra of the primitive unit cell point in different directions (up-down structure), and in the second case the tetrahedra point in the same direction (up-up structure).

To start the determination of the up-down structure, we consider the lattice constants of the $K_2SeO_4$ cited in Ref. 20 and the atomic positions of the up-down $K_2SO_4$ hexagonal structure.[33] We build the up-up structure starting from the up-down configuration, by switching the orientation of one of the two tetrahedra. The up-down structure has the $P\bar{3}m1$ space group and the up-up structure has the $P6_3mc$ space group. We perform the full optimization of the structures, allowing the relaxation of the lattice constants and the internal degrees of freedom under symmetry constraints.

The theoretically determined lattice constants for the up-down structure are $a=6.119$ Å, $c=7.944$ Å, with a unit cell volume of 257.50 Å (Ref. 3), while those of the up-up structure are $a=5.912$ Å, $c=9.002$ Å, with a unit cell volume of 272.54 Å (Ref. 3). The $c:a$ ratios are 1.298 and 1.522 for the up-down and up-up structures, respectively. The differences between the two structures are exclusively due to the different orientations of the $SeO_4$ tetrahedra. The energy of the up-up structure is 9 mHa (0.245 eV) per unit cell higher than the energy of the up-down structure.

The experimental lattice constants are $a=6.14$ Å, $c=8.90$ Å. The comparison between the lattice constants of the experimental structure and any of the theoretically determined structures is somehow disappointing. However, we observe that the differences between the theory and experiment are 0.05% for the $a$ of the up-down structure and 1.12% for the $c$ of the up-up structure. When comparing with the theoretical results, we can imagine that the x-ray diffraction "sees" the $a$ and $c$ lattice constants of the up-down and up-up theoretically determined structures, respectively. This fact may be due to a dynamical disorder state of the $SeO_4$ sublattice at high temperature combined with large anharmonic effects, quite reasonable at high temperatures. Such a mechanism has already been proposed to explain some features of the Raman spectra.[34] According to this mechanism, the $SeO_4$ tetrahedra may flip independently between the positions of energy mimima of a double-well potential, the maximum of both lattice constants being adopted by the mean structure, in order to allow all possible orientations of the selenate groups.

The atomic positions are summarized in the Table I, while Table II lists the Se–O distances and the O-Se-O angles for the $SeO_4$ tetrahedra. The geometry of the $SeO_4$ tetrahedra is very similar in the four structures. In the hexagonal case, the differences between the up-down and up-up structures are less than 1% in Se-O bond lengths and about 2.6° in O-Se-O angles. The deviation from an ideal tetrahedron is more pronounced in the up-down structure.

### B. Orthorhombic structure

The space group of the orthorhombic structure is $Pnam$. The experimental lattice constants[7,35] of the orthorhombic structure are $a=7.661$, $b=10.466$, and $c=6.003$ Å, and the

TABLE I. Theoretical atomic reduced coordinates for the high-$T$ hexagonal up-down (UD) and up-up (UU) structures.

| Atom | $x/a$ | $y/b$ | $z/c$ |
|---|---|---|---|
| UD | | | |
| K(1) | 0.0000 | 0.0000 | 0.0000 |
| K(2) | 1/3 | 2/3 | 0.8279 |
| Se | 1/3 | 2/3 | 0.2931 |
| O(1) | 1/3 | 2/3 | 0.4953 |
| O(2) | 0.1896 | 0.8104 | 0.2190 |
| UU | | | |
| K(1) | 0.0000 | 0.0000 | 0.4139 |
| K(2) | 1/3 | 2/3 | 0.6777 |
| Se | 1/3 | 2/3 | 0.2086 |
| O(1) | 1/3 | 2/3 | 0.3887 |
| O(2) | 0.1825 | 0.8175 | 0.1512 |

theoretically determined lattice constants are $a=7.709$, $b=10.383$, and $c=6.425$ Å. The $a$ and $b$ parameters have absolute deviations of less than 1% with respect to the experiment, while the $c$ parameter is larger by about 7% than the experimental data. The orthorhombic structure corresponds to a distorted hexagonal up-down $c\times a\sqrt{3}\times b$ superstructure. The distortion consists mainly in shifts of half of the K $-SeO_4$ chains along the $c$ hexagonal axis by about $c/2$ and of complex displacements of the atoms, mainly K, in the hexagonal (001) plane. The comparison between the theoretically determined up-down hexagonal and orthorhombic structures shows only a small modification of the unit cell volume, 514.27 Å (Ref. 3) for the orthorhombic structure, corresponding to a factor of 1.997 with respect to the up-down structure volume. The lattice constants exhibit larger variations: elongation along the hexagonal $a$ axis of 5.01% and compression along the hexagonal [2 1 0] and [0 0 1] directions of 2.01 and 2.91%, respectively. The gain in energy of the orthorhombic phase with respect to the hexagonal up-down structure is of 23.84 mHa (0.649 eV) per unit cell.

Table III presents the independent internal coordinates of the atoms in the orthorhombic structure and Table II lists the Se-O distances and the O-Se-O angles for the $SeO_4$ tetrahedra. Differences with the experimental data[7,35] are observed at the level of 0.01, better than the results obtained in Ref. 14 using a Gordon-Kim model.

## IV. ELECTRONIC PROPERTIES

### A. Valence electron density

The distribution of the valence electron density reveals the ionic character of the structure: isolated K cations and $SeO_4$ tetrahedral anionic groups can be identified. A cross section through the $SeO_4^{-2}$ group of the experimental orthorhombic *Pbnm* structure (Fig. 1), shows a large amount of charge between the Se and the O atoms: the Se-O bonds are highly covalent. The Se electronic valence is asymetric, and the electronic charge is almost absent between neighboring oxygens, the O-O bond being much weaker than the Se-O bond. The large Se cation pushes away the oxygens, lenghtening the O-O interatomic distance. This facilitates the distortion of the $SeO_4^{-2}$ anionic group, which is an active component of the normal-to-incommensurate phase transition.[12] The $SeO_4$ group differs from other similar tetrahedral molecular anionic groups, like $SiO_4$, where the smaller size of the central cation allows a stronger interaction between oxygens and renders the anionic group much more rigid.

### B. Electronic band structure and density of states

The electronic density of states (DOS) and the electronic band structure along a high-symmetry path in the first Brillouin zone, as calculated for the theoretical up-down hexagonal structure, are represented in Figs. 2(a) and 2(b), respectively. The top of the valence bands is magnified in Fig. 2(c).

TABLE II. Comparison of the geometric parameters of the $SeO_4$ group (Se-O bond distances, in Bohr and O-Se-O angles, in degrees) in the experimental orthorhombic (EO), and the calculated orthorhombic (CO), and hexagonal up-down (UD) and up-up (UU) structures. The numbering of the oxygen atoms is a guide to ease the comparison.

| Parameter | EO | CO | UD | UU |
|---|---|---|---|---|
| Se-O bonds | | | | |
| $Se-O_1$ | 3.089 | 3.055 | 3.037 | 3.064 |
| $Se-O_2$ | 3.104 | 3.085 | 3.085 | 3.079 |
| $Se-O_3$ | 3.104 | 3.085 | 3.085 | 3.079 |
| $Se-O_4$ | 3.113 | 3.087 | 3.085 | 3.079 |
| O-Se-O angles | | | | |
| $O_1-Se-O_2$ | 110.1 | 110.0 | 111.1 | 108.5 |
| $O_1-Se-O_3$ | 110.1 | 110.0 | 111.1 | 108.5 |
| $O_1-Se-O_4$ | 110.9 | 110.5 | 111.1 | 108.5 |
| $O_2-Se-O_3$ | 108.6 | 109.4 | 107.7 | 110.4 |
| $O_2-Se-O_4$ | 108.5 | 108.4 | 107.7 | 110.4 |
| $O_3-Se-O_4$ | 108.5 | 108.4 | 107.7 | 110.4 |

TABLE III. Calculated (this study) and experimental (Refs. 7 and 35) reduced positions of the symmetry-independent atoms in the orthorhombic phase of $K_2SeO_4$.

| Atom | $x/a$ | $y/b$ | $z/c$ |
|---|---|---|---|
| K(1) | | | |
| This study | 0.1662 | 0.0825 | 0.2500 |
| Ref. 7 | 0.1670 | 0.0809 | 0.2500 |
| Ref. 35 | 0.1705 | 0.0843 | 0.2500 |
| K(2) | | | |
| This study | 0.9989 | 0.7085 | 0.2500 |
| Ref. 7 | 0.9983 | 0.7075 | 0.2500 |
| Ref. 35 | 0.9943 | 0.7095 | 0.2500 |
| Se | | | |
| This study | 0.2242 | 0.4168 | 0.2500 |
| Ref. 7 | 0.2222 | 0.4186 | 0.2500 |
| Ref. 35 | 0.2242 | 0.4200 | 0.2500 |
| O(1) | | | |
| This study | 0.2853 | 0.3382 | 0.0425 |
| Ref. 7 | 0.2891 | 0.3413 | 0.0277 |
| Ref. 35 | 0.2931 | 0.3471 | 0.0271 |
| O(2) | | | |
| This study | 0.3199 | 0.5572 | 0.2500 |
| Ref. 7 | 0.3125 | 0.5617 | 0.2500 |
| Ref. 35 | 0.3024 | 0.5644 | 0.2500 |
| O(3) | | | |
| This study | 0.0157 | 0.4339 | 0.2500 |
| Ref. 7 | 0.0092 | 0.4290 | 0.2500 |
| Ref. 35 | 0.0126 | 0.4251 | 0.2500 |

$K_2SeO_4$ is an insulator, with a 3.68 eV 0 K-LDA gap, direct in $\Gamma$. The experimental gap,[36] obtained from absorbtion edge measurements, is of 6.06 to 6.14 eV at room temperature, decreasing linearly with increasing temperature. The interpolated value at 800 K is about 5.42 to 5.60 eV. The theoretical gap is underestimated, as usual in LDA calculations.

The electronic band structure consists of several well-separated groups of flat bands. The electronic charge corresponding to these bands stems either from K $3p$ orbitals, or from $SeO_4$ molecular orbitals. In the case of the $SeO_4$ molecular orbitals we perform an analysis of the hybridization between the different orbitals on the basis of group theory using the irreducible representations of the $\bar{4}3m$ point group (the deviation of the $SeO_4$ group symmetry from the ideal tetrahedral symmetry is not important and does not affect considerably the electron distribution). There are five $s$ orbitals (1 Se4$s$+4 O2$s$) and fifteen $p$ orbitals (3 Se4$p$ +12 O2$p$) in each $SeO_4$ group, which are hybridized and decomposed as $2A_1+T_2$ and $A_1+E+3T_2+T_1$, respectively. There is a perfect correspondence between each of the terms in the decomposition and each group of valence electronic bands (also in one-to-one correspondence with the DOS peaks). The $s$ bands belonging to the $SeO_4$ group lie in the low-energy zone of the valence bands. In order of increasing energy we find the $A_1$, $T_2$, and $A_1$ representations correspond respectively to the first, second, and fourth peaks in the DOS. The $p$ $SeO_4$ bands lie in the high-energy zone of the valence bands and the first conduction bands. They have a bonding character within the valence bands, and an antibonding character within the conduction bands, where they are mixed with different, higher energy, $s$ and $p$ orbitals. The K3$p$ orbitals lie relatively high in energy between the $s$ $SeO_4$ bands, constituting the third peak in the DOS.

The differences between the electronic structure of the orthorhombic and the hexagonal phases, as well as between the two hexagonal phases are quite small: there are some changes in the energy width of the different groups of electronic bands and in the values of the electronic gaps between them. The energy width of the groups of electronic bands are generally larger in the orthorhombic structure than in the hexagonal structures. The values for the orthorhombic structure are closer to the values corresponding to the up-down structure. The up-up structure presents the narrowest ranges of energy spread of the electronic bands. The difference is more important for the $s$ bands belonging to the $SeO_4$ group. The electronic LDA gap is 3.48, 3.68, and 3.36 eV for the experimental orthorhombic, theoretical up-down, and up-up hexagonal structures, respectively. The energy gaps between the different $s$ $SeO_4$ hybrid bands are more important than those between the different $p$ $SeO_4$ hybrid bands. The energy gap between the highest $s$ and lowest $p$ $SeO_4$ hybrid bands is 2.99, 2.81, and 3.09 eV for the experimental orthorhombic,

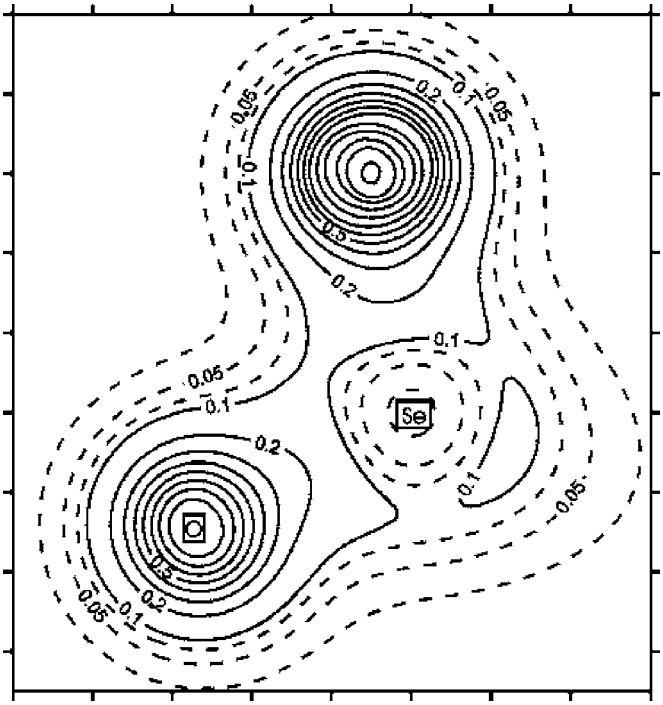


FIG. 1. Cross section (through the $SeO_4$ tetrahedra) of the valence electron density distribution in the experimental orthorhombic structure of $K_2SeO_4$. We remark on the covalent Se-O bonding and the asymmetry of the Se valence electrons. Dashed lines denote the 0.025, 0.05, and 0.075 electron/Bohr (Ref. 3) isodensity contours, while the continuous lines are separated by 0.1 electron/Bohr (Ref. 3). The lateral tick marks are 1 Bohr spaced.

theoretical up-down, and up-up hexagonal structures, respectively. The values of the gaps between the different groups of bands for the experimental orthorhombic structure lie between the values for the two theoretical hexagonal structures.

Our calculations give flatter bands and larger gaps between the different groups of bands than a previous semiempirical LCAO calculations.[22]

## V. DIELECTRIC PROPERTIES

The computed electronic dielectric tensors, $\epsilon^{\infty}$, do not vary significantly between the three structures. The $\epsilon^{\infty}_{11}$ and $\epsilon^{\infty}_{33}$ are 2.37 and 2.43 for the up-down and 2.37 and 2.28 for the up-up structure, respectively. The values for the orthorhombic structure are closer to the up-down than the up-up structure: $\epsilon^{\infty}_{11}=2.40$, $\epsilon^{\infty}_{22}=2.38$, and $\epsilon^{\infty}_{33}=2.36$. Due to the well-known problem in reproducing $\epsilon^{\infty}$ in LDA (Ref. 37) and the previously mentioned gap underestimation it is likely that the above values are overestimated. Further, we calculate the Born effective charges (BEC). They are extremely similar for the three analyzed structures. Table IV lists the BEC of the atoms from the asymmetric unit cell of the orthorhombic structure. All the atoms present deviations from the nominal charges. K presents slightly higher BEC than the nominal charges (+1). Se and O have lower BEC than the nominal charges (+6 and −2, respectively) due to the covalent bonding within the $SeO_4$ tetrahedra.[38] Our calculations give relatively isotropic effective charges for the cations, that are slightly larger than the isotropic effective charges obtained by interpolation of the infrared spectra.[39] The computed BEC of oxygens are instead anisotropic, with an anisotropy less important than the one encountered in the case of the $SiO_4$ tetrahedra from silica.[29]

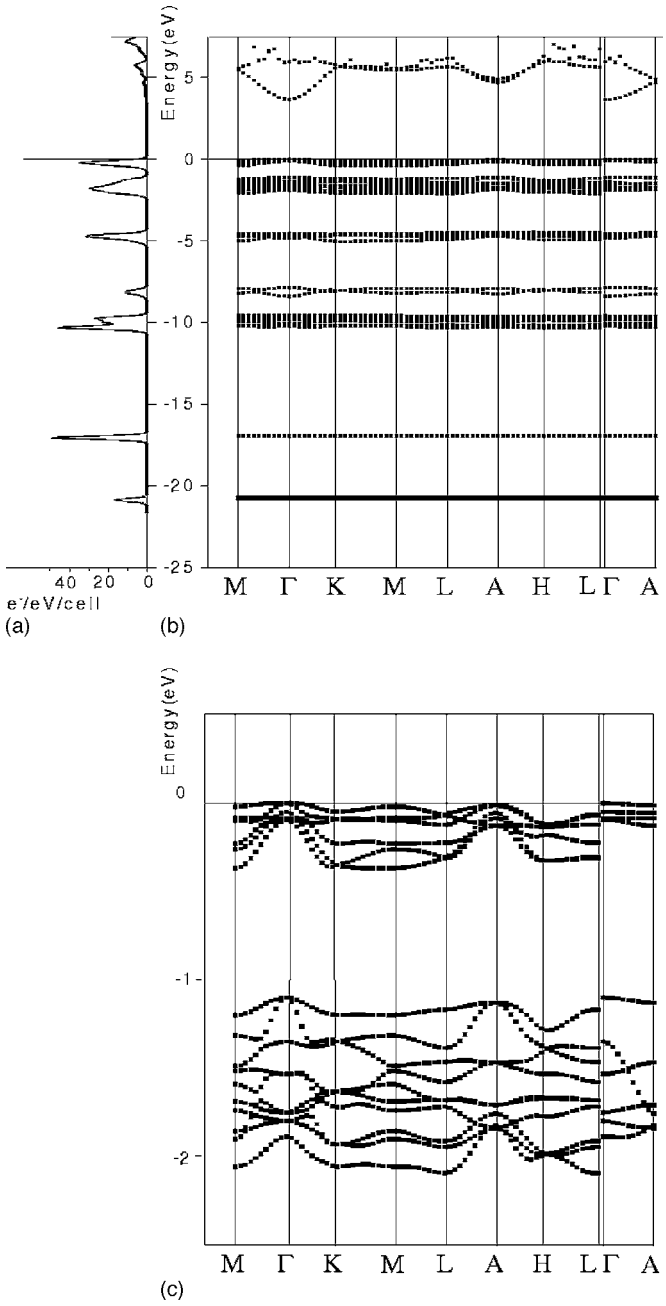


FIG. 2. Electronic band structure and the corresponding electronic density of states for the theoretical up-down hexagonal phase of $K_2SeO_4$. The electronic DOS for the valence bands is shown in (a), the valence bands and the first conduction bands are represented in (b), while the top of the valence bands is magnified in (c).

## VI. ZONE-CENTER LATTICE DYNAMICS

Next, we compute the zone-center vibration modes for the three structures.

TABLE IV. Calculated Born effective charge tensors for the atoms in the orthorhombic *Pnam* structure. The columns (lines) correspond to atomic displacement (polarization) directions. The fourth line, between brakets, gives the eigenvalues of the tensor.

| Atom | | | | |
|---|---|---|---|---|
| | | $x$ | $y$ | $z$ |
| K(1) | $x$ | 1.287 | 0.020 | 0.000 |
| | $y$ | 0.020 | 1.111 | 0.000 |
| | $z$ | 0.000 | 0.000 | 1.115 |
| | | [1.289 | 1.109 | 1.115] |
| K(2) | $x$ | 1.116 | −0.021 | 0.000 |
| | $y$ | −0.021 | 1.283 | 0.000 |
| | $z$ | 0.000 | 0.000 | 1.258 |
| | | [1.285 | 1.258 | 1.114] |
| Se | $x$ | 3.031 | −0.030 | 0.000 |
| | $y$ | −0.030 | 2.923 | 0.000 |
| | $z$ | 0.000 | 0.000 | 2.961 |
| | | [3.039 | 2.961 | 2.915] |
| O(1) | $x$ | −1.099 | 0.134 | 0.221 |
| | $y$ | 0.134 | −1.251 | −0.402 |
| | $z$ | 0.221 | −0.402 | −1.678 |
| | | [−1.995 | −1.025 | −1.009] |
| O(2) | $x$ | −1.252 | −0.379 | 0.000 |
| | $y$ | −0.379 | −1.817 | 0.000 |
| | $z$ | 0.000 | 0.000 | −1.005 |
| | | [−2.007 | −1.062 | −1.005] |
| O(3) | $x$ | −1.978 | 0.134 | 0.000 |
| | $y$ | 0.134 | −1.003 | 0.000 |
| | $z$ | 0.000 | 0.000 | −0.926 |
| | | [−1.996 | −0.985 | −0.926] |

For the hexagonal structures, on the basis of group theory, we obtain decompositions of the vibration modes as $5A_{1g}+1A_{2g}+6E_g+1A_{1u}+7A_{2u}+8E_u$ and $6A_1+1A_2+6B_1+6B_2+7E_1+7E_2$ for the up-down and up-up structures, respectively. The complete list of the vibration mode frequencies, their character, and the LO-TO splitting is shown in Table V for the up-down structure and in Table VI for the up-up structure. The acoustic modes have $A_{2u}+E_u$ and $A_1+E_1$ character in the up-down and up-up structures, respectively. We are not aware of any infrared (IR) or Raman measurements on hexagonal structures.

The up-down hexagonal structure exhibits in the zone center one unstable mode (LO=49.54$i$ cm$^{-1}$ and TO =51.28$i$ cm$^{-1}$), with $E_u$ character. The real space eigendisplacements of this vibration mode are dominated by the O and K(2) movements. They tend to rotate the $SeO_4$ tetrahedra and to displace the K(2) atoms parallel to the Cartesian axes, in the (001) plane.

The up-up hexagonal structure exhibits in the zone center two unstable modes. The first mode has $E_2$ character (59.97$i$ cm$^{-1}$) and the second mode has $E_1$ character (LO =40.02$i$ cm$^{-1}$ and TO=32.62$i$ cm$^{-1}$). They are both dominated by the oxygen displacements that tend to rotate the $SeO_4$ tetrahedra around directions close to $[1\bar{1}0]$ or [110], depending on the tetrahedra position.

TABLE V. Symmetry characteristics and frequencies of the zone-center vibration modes in the hexagonal up-down structure. The $A_{1g}$ and $E_g$ modes are Raman active, the $A_{2u}$ and $E_u$ modes are infrared active and the $A_{2g}$ and $A_{1u}$ are silent.

| Mode | Frequency (cm$^{-1}$) | Mode | TO (cm$^{-1}$) | LO (cm$^{-1}$) |
|---|---|---|---|---|
| $A_{1g}$ | 109 | $A_{2u}$ | 130 | 131 |
| | 153 | | 171 | 250 |
| | 438 | | 220 | 240 |
| | 872 | | 412 | 437 |
| | 961 | | 869 | 873 |
| $A_{2g}$ | 34 | | 956 | 991 |
| $E_g$ | 26 | $E_u$ | 51$i$ | 50$i$ |
| | 92 | | 95 | 101 |
| | 110 | | 104 | 138 |
| | 327 | | 186 | 204 |
| | 413 | | 327 | 327 |
| | 883 | | 408 | 412 |
| $A_{1u}$ | 45 | | 883 | 927 |

TABLE VI. Symmetry characteristics and frequencies of the zone-center vibration modes in the hexagonal up-up structure. The $A_1$, $E_1$, and $E_2$ modes are Raman active, the $A_1$ and $E_1$ modes are infrared active, and the $A_2$, $B_1$, and $B_2$ modes are silent.

| Mode | Frequency ($cm^{-1}$) | Mode | TO ($cm^{-1}$) | LO ($cm^{-1}$) |
|---|---|---|---|---|
| $E_2$ | 60*i* | $A_1$ | 135 | 140 |
| | 54 | | 164 | 197 |
| | 105 | | 413 | 435 |
| | 151 | | 857 | 860 |
| | 414 | | 918 | 955 |
| | 890 | $E_1$ | 40*i* | 33*i* |
| $A_2$ | 109 | | 110 | 125 |
| $B_1$ | 86 | | 149 | 151 |
| | 156 | | 335 | 335 |
| | 163 | | 411 | 413 |
| | 437 | | 890 | 928 |
| | 860 | | | |
| | 948 | | | |
| $B_2$ | 109 | | | |

For the orthorhombic structure we obtain a decomposition of the vibration modes as $13A_g+8B_{1g}+13B_{2g}+8B_{3g}+8A_u+13B_{1u}+8B_{2u}+13B_{3u}$. The $A_u$ modes are silent, all other modes being Raman ($g$ modes) or infrared ($u$ modes) active.

The orthorhombic structure presents two instabilities in Γ. The first unstable mode has $A_u$ character and the second has a $B_{1g}$ character. Both unstable modes represent, in the real space, mixing between alternating displacements of K along the $c$ axis and tetrahedral $E$-type modes of the $SeO_4$ groups. The list of calculated Raman modes for frequencies lower than 300 $cm^{-1}$ is given in Table VII, together with a comparison with experimental[34] and semiempirical calculation[16] results. As we do not have information about the displacement pattern of the different experimental modes, we are not able to establish exactly the correspondence between the calculated and the experimental modes. We consider, besides the mode symmetry, the absolute value of the mode frequency as the criterion to build this correspondence, and we try to assign each computed value to the closest experimental value. This procedure ensures, for most of the modes, absolute deviations on the order of 10 $cm^{-1}$. However, we must consider the 40 $cm^{-1}$ $B_{2g}$ mode as a soft mode, that appears in the experiments, at room temperature, at 119 or 146 $cm^{-1}$.

TABLE VII. Symmetry characteristics and frequencies of the $g$ modes in the orthorhombic structure (low-frequency part of the spectrum, below 300 $cm^{-1}$). The frequencies are expressed in $cm^{-1}$.

| Mode | Theoretical (This study) | Experimental (Ref. 34) | Semiempirical (Ref. 16) |
|---|---|---|---|
| $A_g$ | 52 | 41 | 43 |
| | 73 | 75 | 88 |
| | 92 | 97 | 94 |
| | 105 | 105 | 106 |
| | 133 | 121 | 125 |
| | 154 | 144 | 130 |
| | 173 | 162 | 162 |
| $B_{1g}$ | 76.14 | 47 | 81 |
| | 89 | 74 | 88 |
| | 95 | 96 | 102 |
| | 114 | 109 | 128 |
| | 160 | 120 | 146 |
| | 168 | 143 | 152 |
| | 174 | 160 | 162 |
| $B_{2g}$ | 40.8 | | |
| | 50 | 50 | 57 |
| | 75 | 75 | 81 |
| | 93 | 95 | 85 |
| | 133 | 119 | 114 |
| | | 146 | 154 |
| $B_{3g}$ | 13*i* | | |
| | 50 | 44 | 40 |
| | 69 | 75 | 71 |
| | 84 | 93 | 82 |
| | 126 | 119 | 113 |
| | | 142 | 122 |

TABLE VIII. Symmetry characteristics and frequencies of the $g$ modes in the orthorhombic structure (high-frequency part of the spectrum, above 300 $cm^{-1}$). The frequencies and the differencies are expressed in $cm^{-1}$. The comparison with the experiment is based only on the frequency values. The calculated character of the modes is shown.

| Experiment (Ref. 34) | | Our study | Difference |
|---|---|---|---|
| 333 | $A_g$ | 330 | −3 |
| | $B_{1g}$ | 331 | −2 |
| | $B_{3g}$ | 334 | 1 |
| 343 | $B_{2g}$ | 339 | −4 |
| 414 | $B_{3g}$ | 410 | −4 |
| | $A_g$ | 413 | −1 |
| | $B_{1g}$ | 414 | 0 |
| 419 | $B_{2g}$ | 417 | −2 |
| 430 | $A_g$ | 426 | −4 |
| | $B_{2g}$ | 437 | 7 |
| 844 | $A_g$ | 853 | 9 |
| 865 | $B_{2g}$ | 854 | −11 |
| 876 | $A_g$ | 873 | −4 |
| | $B_{3g}$ | 878 | 2 |
| | $B_{1g}$ | 882 | 6 |
| | $B_{2g}$ | 886 | 9 |
| 906 | $A_g$ | 926 | 20 |
| | $B_{2g}$ | 935 | 29 |

According to this scheme, our results are in a better agreement with the experiment than the data obtained by the semiempirical rigid-ion calculation.[16] The higher frequency modes are listed in Table VIII. With the exception of the two highest modes, the absolute deviations from the experimental values are on the order of 10 $cm^{-1}$.

The calculated $u$ modes for the orthorhombic structure are listed in the Table IX. All the $A_u$ modes are silent, while all the $B_u$ modes are infrared active. However, some isolated $B_u$ modes do not present a sizeable LO-TO splitting. The LO-TO splitting is observed in $\mathbf{q}\rightarrow\Gamma$ along the [001], [010], and [100] directions for the $B_{1u}$, $B_{2u}$, and $B_{3u}$ modes, respectively. Our calculated results, with several exceptions, are in good agreement with the experimental data,[39] as shown in Table IX.

## VII. PHONON BAND DISPERSION IN THE HEXAGONAL PHASES

The two hexagonal structures present similar dispersion bands for the high-frequency modes. Figures 3 and 4 show the dispersion of the phonon bands along the Γ−K−H-A-Γ path through the Brillouin zone for the up-down and up-up structures, respectively. The dispersion of the low-frequencies modes is presented in detail along the Γ-M-L-A-Γ path. In both structures there are four groups of phonon bands. The high-frequency modes, above 250 $cm^{-1}$, are weakly dispersive, and the lattice modes, below 250 $cm^{-1}$ are more dispersive. Both structures present several unstable phonons in the Brillouin zone.

The up-down structure has three modes with imaginary frequencies in L, a point which corresponds to a doubling of the unit cell. An unstable phonon mode appears also in M, and originates from an optical mode with positive frequency in Γ that becomes unstable along the Γ-M line. This mode may participate to the hexagonal-orthorhombic phase transition. The lowest unstable band along K-H-A is weakly dispersive while along M-L-A is highly dispersive. The up-up structure is characterized by several unstable phonon branches which are weakly dispersive along K-H and M-L. The lowest unstable modes are found in M and along the M-L line. The different low-temperature structures can be obtained by the condensation of the unstable phonons at the zone boundary in the up-down and/or up-up hexagonal structures.

## VIII. SUMMARY

We report the ground-state characterization of the hexagonal and orthorhombic phases of $K_2SeO_4$: electronic, structural, dielectric, and dynamical properties, using the local density approximation within the density functional theory as implemented in the code ABINIT.

$K_2SeO_4$ is a mixed ionic-covalent compound, consisting of isolated K cations and $SeO_4$ anionic tetrahedral groups. Within the anionic groups the Se and O are covalently bonded. $K_2SeO_4$ is an insulator, with a 3.67 eV 0 K-LDA gap. The electronic band structure is formed of flat bands, whose electronic charge stems from K4$p$ orbitals or from hybrid Se+O orbitals.

TABLE IX. Symmetry characteristics and frequencies of the calculated and selected experimental $u$ modes in the orthorhombic structure of $K_2SeO_4$. The $A_u$ modes are silent, while the other modes are infrared active. LO modes are found for $\mathbf{q} \rightarrow \Gamma$ along the [001], [010], and [100] directions for $B_{1u}$, $B_{2u}$, and $B_{3u}$ modes, respectively. The frequencies are expressed in $cm^{-1}$. The second to forth columns give the calculated frequencies, while the fifth to seventh columns give the experimental frequencies. The experimental values are extracted from the data published in Ref. 39.

| Mode | Calculated TO | Calculated LO | Calculated LO-TO | Experimental TO | Experimental LO | Experimental LO-TO |
|---|---|---|---|---|---|---|
| $A_u$ | 38$i$ | | | | | |
| | 59 | | | | | |
| | 71 | | | | | |
| | 85 | | | | | |
| | 117 | | | | | |
| | 325 | | | | | |
| | 403 | | | | | |
| | 878 | | | | | |
| $B_{1u}$ | 64 | 72 | 8 | 56 | 64 | 12 |
| | 76 | 102 | 26 | 115 | 125 | 10 |
| | 129 | 167 | 38 | 139 | 177 | 38 |
| | 324 | 324 | 0 | | | |
| | 403 | 424 | 21 | 401 | 435 | 34 |
| | 880 | 922 | 42 | 875 | 926 | 51 |
| $B_{2u}$ | 61 | 61 | 0 | | | |
| | 99 | 99 | 0 | | | |
| | 105 | 125 | 21 | 104 | 116 | 12 |
| | 156 | 158 | 2 | 134 | 139 | 5 |
| | 168 | 170 | 1 | | | |
| | 176 | 203 | 27 | 149 | 188 | 39 |
| | 339 | 339 | 0 | | | |
| | 407 | 421 | 13 | 408 | 420 | 12 |
| | 422 | 431 | 10 | 423 | 434 | 11 |
| | 852 | 852 | 0 | 841 | 842 | 1 |
| | 878 | 916 | 38 | 872 | 901 | 29 |
| | 928 | 931 | 3 | 904 | 910 | 6 |
| $B_{3u}$ | 101 | 102 | 1 | | | |
| | 107 | 108 | 1 | | | |
| | 110 | 111 | 1 | | | |
| | 128 | 131 | 3 | | | |
| | 158 | 158 | 0 | | | |
| | 168 | 206 | 38 | 149 | 200 | 51 |
| | 333 | 333 | 0 | | | |
| | 413 | 427 | 14 | 414 | 425 | 11 |
| | 428 | 439 | 11 | 427 | 445 | 18 |
| | 851 | 854 | 3 | 839 | 841 | 2 |
| | 915 | 916 | 1 | 893 | 907 | 14 |
| | 919 | 956 | 40 | 909 | 934 | 25 |

We determine the two ideal ordered structures of the hexagonal phase, one with the $SeO_4$ tetrahedra pointing in the same direction, with $P6_3mc$ space group, the up-up structure, and one with the $SeO_4$ tetrahedra pointing in opposite directions, with $P\bar{3}m1$ space group, the up-down structure. We consider the possibility of strong anharmonic effects responsible for the dynamical disorder state of the experiental high-$T$ hexagonal structure. we also analyze the orthorhombic structure. The geometry of the $SeO_4$ tetrahedra is similar for all three structures.

The Born effective charges do not present large anomalies, and confirm the ionic character of the K atoms and the

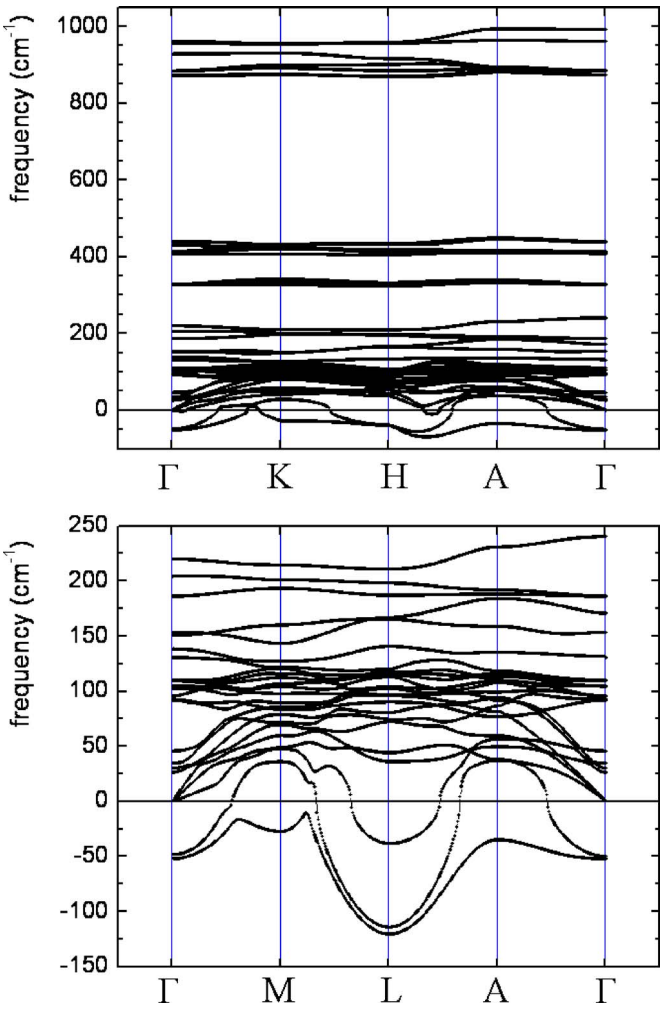


FIG. 3. (Color online) Phonon band dispersion for the hexagonal up-down structure.

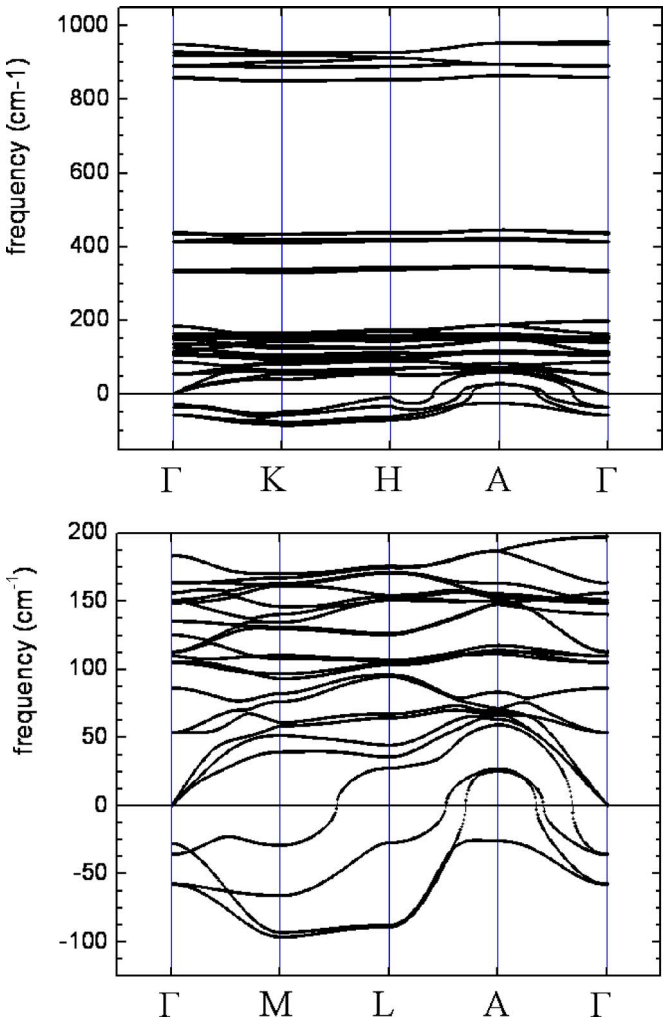


FIG. 4. (Color online) Phonon band dispersion for the hexagonal up-up structure.

covalent bonding within the $SeO_4$ tetrahedral groups.

The hexagonal up-up structure presents two unstable modes in Γ, whose displacement patterns tend to rotate the $SeO_4$ tetrahedra around directions close to [110] or $[\bar{1}10]$. The hexagonal up-down structure presents only one unstable mode in Γ, whose displacement pattern consists of rotations of the $SeO_4$ tetrahedra and displacements of K cations in the (001) plane. The orthorhombic structure presents one *g* and one *u* unstable mode. The agreement with the experimental Raman and infrared modes is often on the order of 10 $cm^{-1}$ or better.

Both hexagonal structures present several unstable phonon modes in the whole Brillouin zone. The lowest mode lie in L in the up-down structure and in M and along the M-L line in the up-up structure.

Our study represents the first *ab initio* investigation of $K_2SeO_4$, the prototype of a large class of dielectric incommensurate materials. Following the review of available studies (see the Introduction), the theoretical determination of the high-temperature structures fill a gap in the literature, while the analysis of the zone-center dynamical properties of the different structures, on a first-principles basis, represents a specific contribution to the understanding of the behavior of this material, and of its phase transitions mechanisms.

## ACKNOWLEDGMENTS

R.C. aknowledges help from computer scientists B. van Renterghem and J.-M. Beuken. X.G. acknowledges financial support from the National Fund for Scientific Research (Belgium). Support also came from the FRFC project No. 2.4556.99 "Simulation numérique et traitement des données."

*E-mail address: r.caracas@gl.ciw.edu

[1] J. D. Axe, M. Iizumi, and G. Shirane, in *Incommensurate Phases in Dielectrics*, edited by R. Blinc and A. P. Levanyuk (North Holland, Amsterdam, 1986) pp. 1–48.
[2] H. Z. Cummins, Phys. Rep. **185**, 211 (1990).
[3] Y. Ishibashi, in *Incommensurate Phases in Dielectrics 2*, edited by R. Blinc and A. P. Levanyuk, (Elsevier Science Publishers, New York, 1986) pp. 49–69.
[4] R. Caracas, J. Appl. Crystallogr. **35**, 120 (2002), http://www.mapr.ucl.ac.be/~crystal/.
[5] M. S. Novikova, R. A. Tamazyan, and I. P. Aleksandrova, Crystallogr. Rep. **40**, 31 (1995).
[6] N. G. Zamkova and V. I. Zinenko, J. Exp. Theor. Phys. **80**, 713 (1995).
[7] N. Yamada and T. Ikeda, J. Phys. Soc. Jpn. **53**, 2555 (1984).
[8] Z. Y. Chen and M. B. Walker, Phys. Rev. Lett. **65**, 1223 (1990).
[9] S. Sawada, M. Takashige, F. Shimizu, H. Suzuki, and T. Yamaguchi, Ferroelectrics **169**, 207 (1995).
[10] K. Inoue, K. Suzuki, A. Sawada, Y. Ishibashi, and Y. Takagi, J. Phys. Soc. Jpn. **46**, 609 (1979).
[11] K. S. Aleksandrov, Crystallogr. Rep. **38**, 67 (1993).
[12] T. M. Chen and R. H. Chen, J. Solid State Chem. **111**, 338 (1994).
[13] M. Iizumi, J. D. Axe, G. Shirane, and K. Shimaoka, Phys. Rev. B **15**, 4392 (1977).
[14] H. M. Lu and J. R. Hardy, Phys. Rev. Lett. **64**, 661 (1990).
[15] Y. Koyama, T. Nagata, and K. Koike, Phys. Rev. B **51**, 12157 (1995).
[16] I. Etxebarria, J. M. Perez-Mato, and A. Criado, Phys. Rev. B **42**, 8482 (1990).
[17] J. M. Perrez-Mato, I. Etxebarria, and G. Madariaga, Phys. Scr., T **39**, 81 (1991).
[18] I. Etxebarria, J. M. Perez-Mato, and G. Madariaga, Phys. Rev. B **46**, 2764 (1992).
[19] I. Etxebarria, R. M. Lynden-Bell, and J. M. Perez-Mato, Phys. Rev. B **46**, 13687 (1992).
[20] V. I. Zinenko and N. G. Zamkova, Phys. Rev. B **57**, 211 (1998).
[21] I. Etxebarria, M. Quilichini, J. M. Perez-Mato, P. Boutrouille, F. J. Zuniga, and T. Breczewski, J. Phys.: Condens. Matter **4**, 8551 (1992).
[22] I. V. Kityk and B. V. Andrievskii, Phys. Status Solidi B **188**, 711 (1995).
[23] P. Hohenberg and W. Kohn, Phys. Rev. **136**, B864 (1964).
[24] W. Kohn and L. J. Sham, Phys. Rev. **140**, A1133 (1965).
[25] X. Gonze, R. Caracas, P. Sonnet, F. Detraux, P. Ghosez, I. Noiret, and J. Schamps, AIP Conf. Proc. No. 535, (AIP, New York, 2000) pp. 13–20.
[26] X. Gonze, J.-M. Beuken, R. Caracas, F. Detraux, M. Fuchs, G.-M. Rignanese, L. Sindic, M. Verstraete, G. Zerah, F. Jollet, M. Torrent, A. Roy, M. Mikami, Ph. Ghosez, J.-Y. Raty, and D. C. Allan, Comput. Mater. Sci. **25**, 478 (2002).
[27] N. Troullier and J. L. Martins, Phys. Rev. B **43**, 1993 (1991). URL: http://www.abinit.org/ABINIT/Psps/LDA_TM/lda.html
[28] W. H. Press, B. P. Flannery, S. A. Teukolsky, and W. T. Vetterling, *Numerical Recipes. The Art of Scientific Computing (FORTRAN Version)* (Cambridge University Press, Cambridge, 1989).
[29] X. Gonze, D. C. Allan, and M. P. Teter, Phys. Rev. Lett. **68**, 3603 (1992).
[30] X. Gonze, Phys. Rev. B **55**, 10337 (1997).
[31] X. Gonze and C. Lee, Phys. Rev. B **55**, 10355 (1997).
[32] S. Baroni, S. de Gironcoli, A. Dal Corso, and P. Giannozzi, Rev. Mod. Phys. **73**, 515 (2001).
[33] A. J. van den Berg and F. Tuinstra, Acta Crystallogr. **B34**, 3177 (1978).
[34] N. E. Massa, F. G. Ullman, and J. R. Hardy, Phys. Rev. B **27**, 1523 (1983).
[35] A. Kalman, J. S. Stephens, and D. W. J. Cruickshank, Acta Crystallogr. **B26**, 1451 (1970).
[36] S. Pacesova, B. Brezina, and L. Jastrabik, Phys. Status Solidi B **116**, 645 (1983).
[37] X. Gonze, Ph. Ghosez, and R. W. Godby, Phys. Rev. Lett. **74**, 4035 (1995).
[38] Ph. Ghosez, J.-P. Michenaud, and X. Gonze, Phys. Rev. B **58**, 6224 (1998).
[39] P. Echegut, F. Gervais, and N. E. Massa, Phys. Rev. B **34**, 278 (1986).